Nano Research
https://doi.org/10.1007/s12274-018-2090-0
Research Article
ISSN 1998-0124
CN 11-5974/O4

Construction of bilayer $PdSe_2$ on epitaxial graphene

En Li[§], Dongfei Wang[§], Peng Fan[§], Ruizi Zhang, Yu-Yang Zhang, Geng Li, Jinhai Mao, Yeliang Wang, Xiao Lin (✉), Shixuan Du, and Hong-Jun Gao (✉)

Institute of Physics & University of Chinese Academy of Sciences, Chinese Academy of Sciences, Beijing 100190, China
[§] *En Li, Dongfei Wang and Peng Fan contributed equally to this work.*

Received: 12 March 2018
Revised: 25 April 2018
Accepted: 7 May 2018

KEYWORDS
two-dimensional materials, transition-metal dichalcogenides, $PdSe_2$, scanning tunneling microscopy/spectroscopy, semiconducting bandgap, nanoribbon

ABSTRACT

Two-dimensional (2D) materials have received significant attention due to their unique physical properties and potential applications in electronics and optoelectronics. Recent studies have demonstrated that exfoliated $PdSe_2$, a layered transition metal dichalcogenide (TMD), exhibits ambipolar field-effect transistor (FET) behavior with notable performance and good air stability, and thus serves as an emerging candidate for 2D electronics. Here, we report the growth of bilayer $PdSe_2$ on a graphene-SiC(0001) substrate by molecular beam epitaxy (MBE). A bandgap of 1.15 ± 0.07 eV was revealed by scanning tunneling spectroscopy (STS). Moreover, a bandgap shift of 0.2 eV was observed in $PdSe_2$ layers grown on monolayer graphene as compared to those grown on bilayer graphene. The realization of nanoscale electronic junctions with atomically sharp boundaries in 2D $PdSe_2$ implies the possibility of tuning its electronic or optoelectronic properties. In addition, on top of the $PdSe_2$ bilayers, $PdSe_2$ nanoribbons and stacks of nanoribbons with a fixed orientation have been fabricated. The bottom-up fabrication of low-dimensional $PdSe_2$ structures is expected to enable substantial exploration of its potential applications.

1 Introduction

Since the discovery of graphene, investigations into two-dimensional (2D) atomic crystal materials have advanced rapidly [1–3]. Among all the 2D materials fabricated and studied so far, layered transition metal dichalcogenides (TMDs) have emerged as an important class of 2D materials with fascinating physical properties and potential applications [4, 5] due to their sizable bandgaps and strong spin–orbit and spin–valley coupling effects [6, 7]. Interesting properties emerged when TMD bulk crystals were thinned down to the 2D limit. For example, indirect-to-direct bandgap transitions occurred when bulk $MoSe_2$ or WSe_2 was thinned down to single layers [8, 9], and a large exciton binding energy of 0.55 eV has been observed in monolayer $MoSe_2$ [10]. Single layer $PtSe_2$ exhibits semiconducting properties [11]. Therefore, developing

Address correspondence to Xiao Lin, xlin@ucas.ac.cn; Hong-Jun Gao, hjgao@iphy.ac.cn

experimental techniques to fabricate 2D materials is important.

$PdSe_2$ is a type of layered TMD known for its unique crystal structure and remarkable layer-dependent electronic structure. In contrast to the well-studied 1T, 2H, and 1T′ structures of 2D TMDs [4, 12], $PdSe_2$ has a puckered pentagonal structure with an orthorhombic lattice [13], which leads to novel properties such as the anisotropic behavior in field-effect transistors (FETs) [14, 15]. 2D materials with puckered pentagonal structures, such as penta-graphene [16] and penta-SnX_2 (X = S, Se, or Te) [17, 18], have been theoretically predicted to have unusual physical properties but remain unexplored experimentally. Under high pressure, bulk $PdSe_2$ undergoes a structural transition and shows superconductivity [19]. Furthermore, first-principles calculations predict a semiconducting behavior in $PdSe_2$ with a thickness-dependent bandgap from 0.03 eV in the bulk to 1.43 eV in monolayers [20], which has recently been confirmed by optical absorption spectroscopy [15]. Moreover, FETs based on few-layer $PdSe_2$ display intrinsic ambipolar characteristics with a high carrier mobility of 158 or 216 $cm^2 \cdot V^{-1} \cdot s^{-1}$ and high on/off ratio [14, 15]. In addition, $PdSe_2$ is stable in air [15]. Its unique pentagonal structure and notable FET performance with good atmospheric stability make $PdSe_2$ intriguing for applications in electronic and photoelectric devices. Nevertheless, to our knowledge, $PdSe_2$ thin layers have mainly been fabricated by mechanical exfoliation from the bulk crystal [14, 15, 21]. Epitaxial growth of atomically thin $PdSe_2$ layers or $PdSe_2$-based nanostructures has not been realized by either chemical vapor deposition (CVD) or molecular beam epitaxy (MBE). Meanwhile, nanoribbons of 2D materials, especially TMDs, have been theoretically predicted to show intriguing properties, such as magnetic properties [22], strong excitonic correlation effects [23], sizable valley pump effects [24] and high-performance thermoelectric effects [25]. However, bottom-up fabrication of TMD nanoribbons remains challenging and only limited successes have been achieved [26, 27].

In the present work, by using epitaxial graphene on SiC(0001) as a substrate, we report the fabrication of bilayer $PdSe_2$ based on MBE. The structural and electronic properties of the $PdSe_2$ layers are investigated by scanning tunneling microscopy (STM) and scanning tunneling spectroscopy (STS) combined with first-principles calculations. The bandgap of $PdSe_2$ layers and the band modulation effect by the substrate have been investigated by STS measurements. Moreover, $PdSe_2$ nanoribbons are also observed to grow on top of the 2D layers.

2 Results and discussion

The atomic structure of bulk $PdSe_2$ is shown in Fig. 1(a). Bulk $PdSe_2$ crystallizes in an orthorhombic structure (space group *Pbca*) with a unit cell of a = 5.7457 Å, b = 5.8679 Å, and c = 7.6976 Å [13]. The 2D Se–Pd–Se layers are stacked by van der Waals (vdW) interactions and one unit cell (1UC) contains two $PdSe_2$ layers due to relative displacement of the two adjacent layers in the b direction. The atomic structure of monolayer $PdSe_2$ is shown in Fig. 1(b). Compared to the structures of the widely investigated T- or H-phase TMDs, in which each transition metal atom binds to six chalcogen atoms, each Pd atom in $PdSe_2$ binds to four Se atoms, forming a unique puckered pentagonal structure.

Figure 1(c) (as well as Fig. S1 in the Electronic Supplementary Material (ESM)) shows an STM topographic image of $PdSe_2$ layers grown on a graphene/SiC(0001) substrate, with corresponding X-ray photoelectron spectroscopy (XPS) results shown in Fig. S2 in the ESM. The rectangular shape of the 2D islands in the STM image is consistent with the orthorhombic symmetry of $PdSe_2$. The apparent height of the island is ~ 7.8 Å (Fig. 1(d)), suggesting that the islands consist of bilayer $PdSe_2$ instead of monolayer. We have tried to adjust the experimental conditions, e.g., decreasing the dosing of the precursors; however, monolayer $PdSe_2$ was never found. Density functional theory (DFT) calculations show that the interlayer interaction in $PdSe_2$ is significantly stronger than that in other vdW stacking layered materials such as graphite and MoS_2 (see Table S1 in the ESM). This may explain the bilayer growth mode. More experiments and calculations are needed for an in-depth understanding. We note that a recent study using scanning transmission electron microscopy shows that, driven by the creation of Se vacancies under electron irradiation, bilayer $PdSe_2$ will melt into one layer, forming the new Pd_2Se_3 structure

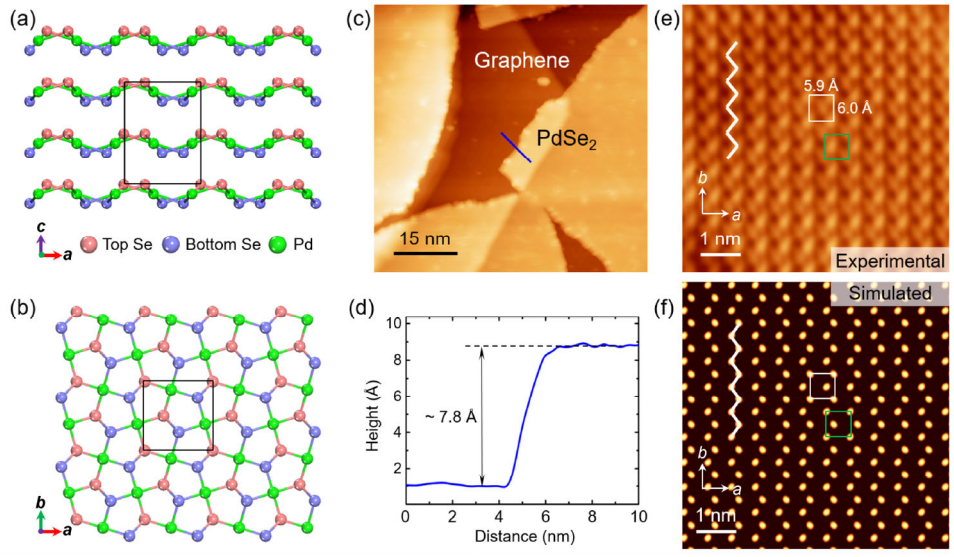

Figure 1 Bilayer $PdSe_2$ formed on a graphene substrate. (a) Side view of the atomic structure of bulk $PdSe_2$. The unit cell consists of two $PdSe_2$ layers, as indicated by the rectangle. (b) Top view of the crystal structure of single layer $PdSe_2$ showing pentagonal rings. The rectangle indicates the unit cell in a monolayer. (c) An STM topographic image (−3.0 V, 100 pA) of $PdSe_2$ islands on graphene on SiC(0001). (d) The line profile along the blue line in (c), showing that the apparent height of the island is ~ 7.8 Å. (e) An atomic-resolution STM image (1.0 V, 100 pA) of the $PdSe_2$ islands. Two sublattices in the top Se layer are marked with white and green rectangles. (f) Simulated STM image (1.0 V) of bilayer $PdSe_2$, consistent with the experimental observation in (e). White lines denote zigzag rows in the atomic-resolution image.

[21]. The demonstration of the fabrication technique of bilayer $PdSe_2$ makes it possible to create and explore more properties of this new 2D phase.

Figure 1(e) shows the atomic-resolution STM image of the $PdSe_2$ islands, which agrees well with the simulated STM image of bilayer $PdSe_2$ (Fig. 1(f)). Both constant-current and simulated STM images reveal zigzag rows along the *b* direction (white zigzag line in Figs. 1(e) and 1(f)), which correspond to the topmost plane of Se atoms in the $PdSe_2$ sandwich-type structure. The surface structure yields two mirror-symmetric rectangle sublattices, as highlighted by white and green rectangles in Figs. 1(e) and 1(f), similar to the puckered surface structure of black phosphorus [28, 29]. The measured lattice constants of the as-fabricated bilayer $PdSe_2$ are a = 5.9 Å and b = 6.0 Å, slightly larger than the bulk values (a = 5.75 Å and b = 5.87 Å). Note that Oyedele et al. [15] reported that the optimized bulk lattice constants obtained via optimized Perdew, Burke, and Ernzerhof (optPBE) are a = 5.85 Å and b = 5.99 Å, which agree well with our results.

We then investigated the electronic structure of the fabricated bilayer-$PdSe_2$ islands through a combination of DFT calculations and STS experiments. Figure 2(a) displays the band structure of the bilayer-$PdSe_2$ calculated at the PBE level, showing an indirect bandgap of 0.94 eV. As shown in Fig. 2(b), the experimental dI/dV spectrum of the bilayer-$PdSe_2$ was plotted using a linear scale (black) for the y-axis on the left side and a logarithmic scale (green) on the right. The bandgap and positions of the valence band maximum (VBM) and conduction band minimum (CBM) are clearly shown. To better determine the width of the bandgap, we show the statistical distributions of the results from 121 individual tunneling spectra measured from different locations as illustrated in Fig. 2(c). The mean value of the bandgap of the $PdSe_2$ bilayer is 1.15 eV while the standard deviation (σ) is 0.07 eV, which is a little larger than the calculated result (0.94 eV). Recent work shows the measured bandgap of exfoliated bilayer $PdSe_2$ by optical absorption spectroscopy is less than 1.0 eV [15]. The difference between our STS result and the optical measurement result might be attributed to the excitonic effects in 2D semiconducting TMDs such as WSe_2 [9] and $MoSe_2$ [10].

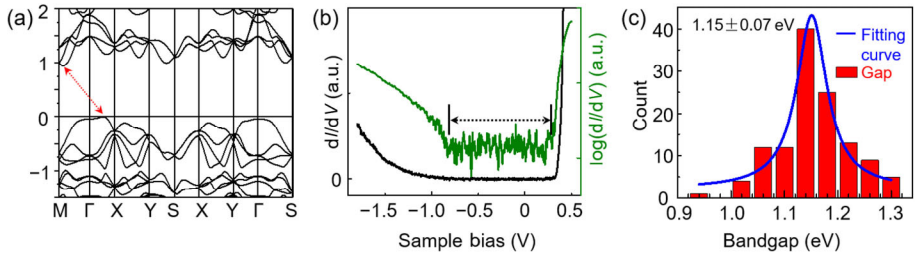

Figure 2 Electronic structure of the bilayer $PdSe_2$ on a graphene substrate. (a) Calculated band structure of bilayer $PdSe_2$ using the PBE method. The red arrow indicates the lowest energy transitions between the VBM and CBM. The Fermi energy is set at zero. (b) Scanning tunneling spectrum of bilayer $PdSe_2$ showing the bandgap. The logarithm of the dI/dV tunneling spectrum is shown in green to accentuate the noise floor within the gapped region. (c) Statistical distribution (from 121 individual dI/dV spectra) of the bandgap measured for bilayer $PdSe_2$, resulting in a mean bandgap of 1.15 ± 0.07 eV.

Both bilayer graphene (BLG) and monolayer graphene (MLG) can be formed on SiC(0001) surfaces; surface morphology and STS are often used to identify BLG and MLG regions [30]. In our experiments, $PdSe_2$ layers were found growing continuously across BLG-MLG steps as shown in Fig. 3(a) and the low-magnification image in Fig. S3(a) in the ESM. A high-magnification STM image (Fig. 3(b)) of the area indicated by the black rectangle in Fig. 3(a) confirms the continuity of the $PdSe_2$ layer.

We carried out STS measurements on the $PdSe_2$ layer. As shown in Fig. 3(c), a series of tunneling spectra were taken along the dotted black line in Fig. 3(a). The numbers on the spectra refer to their position in the complete set, in which spectra were acquired every 1.25 nm. From the $PdSe_2$ layer on top of the BLG to that on the MLG area, a downward band bending can be clearly resolved, as indicated by the dashed black line in Fig. 3(c). This band bending starts at spectrum #15, the first dot in $PdSe_2$ on MLG/SiC, and finally tends towards stability with a shift of ~ 0.2 eV after 5 nm. Two individual spectra of $PdSe_2$ on BLG and MLG from another experiment are shown in Fig. 3(d). The dI/dV curves of $PdSe_2$ on BLG and MLG are very similar except for a clear shift of 0.2 eV, which is likely due to the substrate doping effect. Typically, the CBM and VBM of $PdSe_2$ sheets on BLG/SiC are located at 0.31 and −0.84 eV, respectively. However, on MLG/SiC substrate, the CBM and VBM of $PdSe_2$ sheets moved to 0.12 and −1.06 eV, respectively.

This result is further evidenced by a dI/dV mapping measurement. Figure 3(e) displays the STM topography image of bilayer-$PdSe_2$ across the BLG-MLG step edge, showing the apparent height difference. However, the simultaneously acquired dI/dV signal taken at 0.20 V sample bias has a reversed contrast, as shown in Fig. 3(f), owing to the lower local density of states at 0.20 eV for $PdSe_2$ on the BLG region compared to that on MLG. The dI/dV mapping confirms the shift of the $PdSe_2$ band structure with an atomically sharp boundary.

Increasing numbers of graphene layers on SiC weaken the charge transfer from the substrate, resulting in varied electronic properties of the as-fabricated bilayer-$PdSe_2$. $PdSe_2$ sheets can grow continuously on mono- and bi- layer graphene. Therefore, we have realized nanoscale and atomically sharp electronic junctions in 2D $PdSe_2$ layers by controlling the number of underlying graphene layers. The in-plane band modulations of $PdSe_2$ layers make it possible to tune electronic and optoelectronic properties of 2D TMD semiconductors, or even build p–n junctions for potential applications in photovoltaics and electronics.

Besides 2D islands, one-dimensional (1D) $PdSe_2$ nanostructures form on top of the $PdSe_2$ islands and the orientations of these nanostructures follow one of the rectangular island's edges as shown in Figs. S3(a) and S4(a) in the ESM, suggesting an epitaxial growth mode. To understand the 1D $PdSe_2$ nanostructures, we fabricated samples with lower coverages. $PdSe_2$ nanoribbons with ~ 5 nm widths were observed on the islands as shown in Fig. 4(a). An atomic-resolution image of a nanoribbon is shown in Fig. 4(b), confirming the same surface structure and epitaxial growth as the underlying $PdSe_2$ islands.

We measured the apparent heights of the nanoribbons

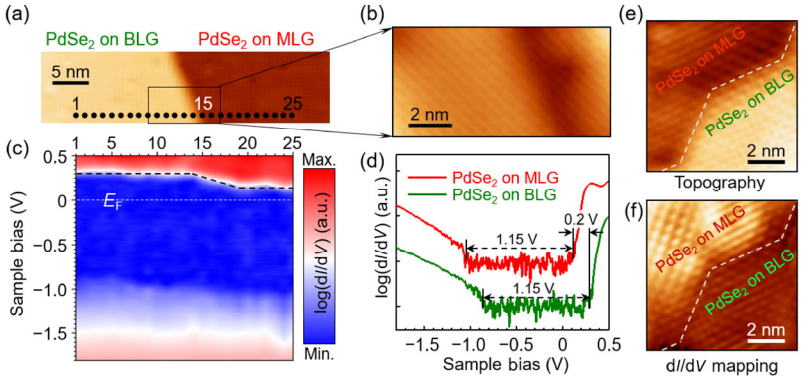

Figure 3 Electronic properties of $PdSe_2$ bilayers on MLG and BLG on SiC(0001). (a) STM image (2.0 V, 100 pA) showing one $PdSe_2$ bilayer across the BLG-MLG substrate. (b) High-magnification STM image (0.5 V, 100 pA) of the black rectangle in (a), revealing the continuity of the $PdSe_2$ layer above the BLG-MLG step edge. (c) d*I*/d*V* spectra plotted in a 2D color mapping in logarithmic scale. 25 curves were measured with an interval of 1.25 nm along the path shown in (a). (d) d*I*/d*V* spectra of one $PdSe_2$ island on BLG (green) and MLG (red) show the bandgap shift clearly. The curves are vertically offset for clarity. (e) An STM topographic image (0.2 V, 100 pA) of a $PdSe_2$ island across BLG-MLG. (f) Corresponding d*I*/d*V* mapping image (0.2 V, 100 pA) of (e).

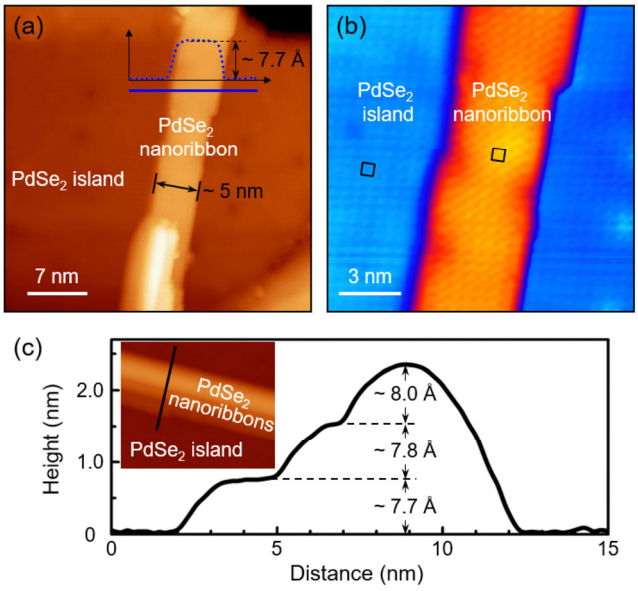

Figure 4 $PdSe_2$ nanoribbons growing epitaxially on $PdSe_2$ islands. (a) An STM topographic image (1.0 V, 100 pA) of a bilayer-$PdSe_2$ nanoribbon on a bilayer-$PdSe_2$ island. (b) An atomic resolution STM image (1.0 V, 100 pA) of a bilayer-$PdSe_2$ nanoribbon showing the same surface structure and orientation as the underlying $PdSe_2$ island. (c) Line profiles across multilayer $PdSe_2$ nanoribbons, showing the same (~ 7.7 Å) apparent height of each layer.

located on different layers as shown in Figs. 4(a) and 4(c). They have almost identical heights of ~ 7.7 Å, in good agreement with bilayer $PdSe_2$, indicating that the first bilayer-$PdSe_2$ nanoribbon grows on top of the bilayer-$PdSe_2$ 2D island and the second and third bilayer-$PdSe_2$ nanoribbons grow on the first nanoribbon sequentially. Given higher precursor dosages, the nanoribbons can stack together to form multilayers. In such cases, the building blocks are always bilayer nanoribbons, as shown in Fig. 4(c). The strict bilayer stacking behavior suggests again the stable nature of the bilayer structure of $PdSe_2$, which corresponds to one unit cell of the bulk.

As shown in Fig. S4(a) in the ESM, the orientation of the nanoribbon follows the direction of one edge of the island and Fig. S4(b) in the ESM shows that the direction of that edge is the same as the direction of the zigzag rows, which is along the *b* direction as we can see from Figs. 1(e) and 1(f). The anisotropic surface structure of $PdSe_2$ may lead to faster nucleation of the second $PdSe_2$ layer in the *b* direction with respect to *a*, and thus result in the formation of 1D nanoribbons. This is in clear contrast to the growth behavior of $PdSe_2$ on the graphene surface, which has a different symmetry than $PdSe_2$ and would therefore lead to isotropic growth of the 2D $PdSe_2$ islands. Since 1D nanoribbons of TMDs are a class of highly desirable materials owing to their predicted unusual properties, the bottom-up fabrication of $PdSe_2$ nanoribbons gives researchers an opportunity to explore the electronic properties of the TMD nanoribbons family.

3 Conclusions

In summary, we have demonstrated the MBE growth of bilayer $PdSe_2$ islands on bilayer and monolayer

graphene on SiC(0001). A bandgap of 1.15 ± 0.07 eV was revealed by STS measurement. Moreover, a 0.2 eV bandgap shift was observed in $PdSe_2$ layers grown on monolayer graphene as compared to those grown on bilayer graphene on SiC. The realization of nanoscale and atomically sharp electronic junctions in $PdSe_2$ sheets suggests the possibility of tuning the electronic or optoelectronic properties for potential technological applications. In addition, structurally well-defined $PdSe_2$ nanoribbons have been achieved on $PdSe_2$ islands and the nanoribbons exhibit stacking growth with a fixed orientation. The bottom-up fabrication of 1D $PdSe_2$ nanoribbons is expected to enable substantial exploration of 1D TMDs.

4 Methods

4.1 Experimental details

Experiments were carried out in an ultrahigh vacuum STM system, with a base pressure of 2.0×10^{-10} mBar, equipped with standard MBE capabilities for *in-situ* sample preparation. A nitrogen-doped 6H-SiC(0001) wafer (0.1 Ω·cm) was graphitized by flashing to 1,550 K, leading to a graphene terminated surface [31, 32] as the substrate for the MBE growth of $PdSe_2$. The quality of the graphene was evaluated by low-energy electron diffraction (LEED) and STM. High-purity Pd (99.95%, Alfa Aesar) and Se (99.999%, Alfa Aesar) sources were simultaneously evaporated from an electron-beam evaporator and a standard Knudsen diffusion cell with a flux ratio of ~ 1:10, while the substrate was maintained at 500 K during the growth process. After growth, the sample was transferred to STM chambers for STM/STS measurements. STS measurements were performed at 4.2 K by using a lock-in technique with a 20 mV_{rms} sinusoidal modulation at a frequency of 987.5 Hz. dI/dV spectra on a Au(111) substrate were used as an STS reference for tip calibration.

4.2 Theoretical calculation details

First-principles calculations were performed within the Vienna *ab initio* simulation package (VASP) [33], version 5.4.1, using the projector augmented-wave (PAW) method [34]. A plane-wave basis set was used, with a kinetic energy cutoff of 420 eV. Electron exchange and correlation effects were treated using the generalized gradient approximation (GGA) functional of PBE [35]. $PdSe_2$ bilayers were modeled using a periodic 1 × 1 slab geometry with a vacuum thickness of 15 Å. All the atoms were allowed to relax along the calculated forces of less than 0.01 eV·Å^{-1}. A 21 × 21 × 1 Monkhorst-Pack [36] *k*-point mesh was used to sample the Brillouin zone. The simulated STM images were generated using the Tersoff-Hamann approximation [37].

Acknowledgements

We acknowledge the financial support from the National Natural Science Foundation of China (Nos. 61390501, 61622116 and 61471337), the Chinese Academy of Sciences (Nos. XDPB0601 and XDPB0801) and the CAS Pioneer Hundred Talents Program. Y. Y. Z. would also thank Beijing Nova Program (No. Z181100006218023). A portion of the research was performed in CAS Key Laboratory of Vacuum Physics.

Electronic Supplementary Material: Supplementary material (additional information on bilayer $PdSe_2$ formed on monolayer graphene and bilayer graphene substrate, orientation of the nanoribbons on $PdSe_2$ islands) is available in the online version of this article at https://doi.org/10.1007/s12274-018-2090-0.

References

[1] Jariwala, D.; Davoyan, A. R.; Wong, J.; Atwater, H. A. Van der Waals materials for atomically-thin photovoltaics: Promise and outlook. *ACS Photonics* **2017**, *4*, 2962–2970.

[2] Novoselov, K. S.; Mishchenko, A.; Carvalho, A.; Neto, A. H. C. 2D materials and van der Waals heterostructures. *Science* **2016**, *353*, aac9439.

[3] Pan, Y.; Zhang, L. Z.; Huang, L.; Li, L. F.; Meng, L.; Gao, M.; Huan, Q.; Lin, X.; Wang, Y. L.; Du, S. X. et al. Construction of 2D atomic crystals on transition metal surfaces: Graphene, silicene, and hafnene. *Small* **2014**, *10*, 2215–2225.

[4] Chhowalla, M.; Shin, H. S.; Eda, G.; Li, L.-J.; Loh, K. P.; Zhang, H. The chemistry of two-dimensional layered transition metal dichalcogenide nanosheets. *Nat. Chem.* **2013**, *5*, 263–275.

[5] Wang, Q. H.; Kalantar-Zadeh, K.; Kis, A.; Coleman, J. N.; Strano, M. S. Electronics and optoelectronics of two-dimensional transition metal dichalcogenides. *Nat. Nanotechnol.* **2012**, *7*, 699–712.

[6] Xu, X. D.; Yao, W.; Xiao, D.; Heinz, T. F. Spin and pseudospins in layered transition metal dichalcogenides. *Nat. Phys.* **2014**, *10*, 343–350.

[7] Liu, G.-B.; Xiao, D.; Yao, Y. G.; Xu, X. D.; Yao, W. Electronic structures and theoretical modelling of two-dimensional group-VIB transition metal dichalcogenides. *Chem. Soc. Rev.* **2015**, *44*, 2643–2663.

[8] Zhang, Y.; Chang, T.-R.; Zhou, B.; Cui, Y.-T.; Yan, H.; Liu, Z. K.; Schmitt, F.; Lee, J.; Moore, R.; Chen, Y. L. et al. Direct observation of the transition from indirect to direct bandgap in atomically thin epitaxial $MoSe_2$. *Nat. Nanotechnol.* **2014**, *9*, 111–115.

[9] Zhang, Y.; Ugeda, M. M.; Jin, C. H.; Shi, S.-F.; Bradley, A. J.; Martín-Recio, A.; Ryu, H.; Kim, J.; Tang, S. J.; Kim, Y. et al. Electronic structure, surface doping, and optical response in epitaxial WSe_2 thin films. *Nano Lett.* **2016**, *16*, 2485–2491.

[10] Ugeda, M. M.; Bradley, A. J.; Shi, S.-F.; da Jornada, F. H.; Zhang, Y.; Qiu, D. Y.; Ruan, W.; Mo, S.-K.; Hussain, Z.; Shen, Z.-X. et al. Giant bandgap renormalization and excitonic effects in a monolayer transition metal dichalcogenide semiconductor. *Nat. Mater.* **2014**, *13*, 1091–1095.

[11] Wang, Y. L.; Li, L. F.; Yao, W.; Song, S. R.; Sun, J. T.; Pan, J. B.; Ren, X.; Li, C.; Okunishi, E.; Wang, Y. Q. et al. Monolayer $PtSe_2$, a new semiconducting transition-metal-dichalcogenide, epitaxially grown by direct selenization of Pt. *Nano Lett.* **2015**, *15*, 4013–4018.

[12] Kolobov, A. V.; Tominaga, J. *Two-Dimensional Transition-Metal Dichalcogenides*; Springer: Switzerland, 2016.

[13] Soulard, C.; Rocquefelte, X.; Petit, P.-E.; Evain, M.; Jobic, S.; Itié, J.-P.; Munsch, P.; Koo, H.-J.; Whangbo, M.-H. Experimental and theoretical investigation on the relative stability of the PdS_2- and pyrite-type structures of $PdSe_2$. *Inorg. Chem.* **2004**, *43*, 1943–1949.

[14] Chow, W. L.; Yu, P.; Liu, F. C.; Hong, J. H.; Wang, X. L.; Zeng, Q. S.; Hsu, C. H.; Zhu, C.; Zhou, J. D.; Wang, X. W. et al. High mobility 2D palladium diselenide field-effect transistors with tunable ambipolar characteristics. *Adv. Mater.* **2017**, *29*, 1602969.

[15] Oyedele, A. D.; Yang, S. Z.; Liang, L. B.; Puretzky, A. A.; Wang, K.; Zhang, J. J.; Yu, P.; Pudasaini, P. R.; Ghosh, A. W.; Liu, Z.; Rouleau, C. M. et al. $PdSe_2$: Pentagonal two-dimensional layers with high air stability for electronics. *J. Am. Chem. Soc.* **2017**, *139*, 14090–14097.

[16] Zhang, S. H.; Zhou, J.; Wang, Q.; Chen, X. S.; Kawazoe, Y.; Jena, P. Penta-graphene: A new carbon allotrope. *Proc. Natl. Acad. Sci. USA* **2015**, *112*, 2372–2377.

[17] Ma, Y. D.; Kou, L. Z.; Li, X.; Dai, Y.; Heine, T. Room temperature quantum spin Hall states in two-dimensional crystals composed of pentagonal rings and their quantum wells. *NPG Asia Mater.* **2016**, *8*, e264.

[18] Zhang, R.-W.; Liu, C.-C.; Ma, D.-S.; Yao, Y.-G. From node-line semimetals to large-gap quantum spin Hall states in a family of pentagonal group-IVA chalcogenide. *Phys. Rev. B* **2018**, *97*, 125312.

[19] ElGhazali, M. A.; Naumov, P. G.; Mirhosseini, H.; Süß, V.; Müchler, L.; Schnelle, W.; Felser, C.; Medvedev, S. A. Pressure-induced superconductivity up to 13.1 K in the pyrite phase of palladium diselenide $PdSe_2$. *Phys. Rev. B* **2017**, *96*, 060509.

[20] Sun, J. F.; Shi, H. L.; Siegrist, T.; Singh, D. J. Electronic, transport, and optical properties of bulk and mono-layer $PdSe_2$. *Appl. Phys. Lett.* **2015**, *107*, 153902.

[21] Lin, J. H.; Zuluaga, S.; Yu, P.; Liu, Z.; Pantelides, S. T.; Suenaga, K. Novel Pd_2Se_3 two-dimensional phase driven by interlayer fusion in layered $PdSe_2$. *Phys. Rev. Lett.* **2017**, *119*, 016101.

[22] Li, Y. F.; Zhou, Z.; Zhang, S. B.; Chen, Z. F. MoS_2 nanoribbons: High stability and unusual electronic and magnetic properties. *J. Am. Chem. Soc.* **2008**, *130*, 16739–16744.

[23] Kim, J.; Yun, W. S.; Lee, J. D. Optical absorption of armchair MoS_2 nanoribbons: Enhanced correlation effects in the reduced dimension. *J. Phys. Chem. C* **2015**, *119*, 13901–13906.

[24] An, X.-T.; Xiao, J.; Tu, M. W.-Y.; Yu, H. Y.; Fal'ko, V. I.; Yao, W. Realization of valley and spin pumps by scattering at nonmagnetic disorders. *Phys. Rev. Lett.* **2017**, *118*, 096602.

[25] Zhang, Z. W.; Xie, Y. E.; Peng, Q.; Chen, Y. P. A theoretical prediction of super high-performance thermoelectric materials based on MoS_2/WS_2 hybrid nanoribbons. *Sci. Rep.* **2016**, *6*, 21639.

[26] Cheng, F.; Xu, H.; Xu, W. T.; Zhou, P. J.; Martin, J.; Loh, K. P. Controlled growth of 1D $MoSe_2$ nanoribbons with spatially modulated edge states. *Nano Lett.* **2017**, *17*, 1116–1120.

[27] Chen, Y. X.; Cui, P.; Ren, X. B.; Zhang, C. D.; Jin, C. H.; Zhang, Z. Y.; Shih, C.-K. Fabrication of $MoSe_2$ nanoribbons via an unusual morphological phase transition. *Nat. Commun.* **2017**, *8*, 15135.

[28] Zhang, C. D.; Lian, J. C.; Yi, W.; Jiang, Y. H.; Liu, L. W.; Hu, H.; Xiao, W. D.; Du, S. X.; Sun, L. L.; Gao, H.-J. Surface structures of black phosphorus investigated with scanning tunneling microscopy. *J. Phys. Chem. C* **2009**, *113*, 18823–18826.

[29] Özçelik, V. O.; Azadani, J. G.; Yang, C.; Koester, S. J.; Low, T. Band alignment of two-dimensional semiconductors for designing heterostructures with momentum space matching. *Phys. Rev. B* **2016**, *94*, 035125.

[30] Lauffer, P.; Emtsev, K. V.; Graupner, R.; Seyller, T.; Ley, L.; Reshanov, S. A.; Weber, H. B. Atomic and electronic structure of few-layer graphene on SiC(0001) studied with scanning tunneling microscopy and spectroscopy. *Phys. Rev. B* **2008**, *77*, 155426.

[31] Wang, Q. Y.; Zhang, W. H.; Wang, L. L.; He, K.; Ma, X. C.; Xue, Q. K. Large-scale uniform bilayer graphene prepared by vacuum graphitization of 6H-SiC(0001) substrates. *J. Phys.: Condens. Matter* **2013**, *25*, 095002.

[32] Riedl, C.; Starke, U.; Bernhardt, J.; Franke, M.; Heinz, K. Structural properties of the graphene-SiC(0001) interface as a key for the preparation of homogeneous large-terrace graphene surfaces. *Phys. Rev. B* **2007**, *76*, 245406.

[33] Kresse, G.; Furthmüller, J. Efficient iterative schemes for *ab initio* total-energy calculations using a plane-wave basis set. *Phys. Rev. B* **1996**, *54*, 11169–11186.

[34] Blöchl, P. E. Projector augmented-wave method. *Phys. Rev. B* **1994**, *50*, 17953–17979.

[35] Perdew, J. P.; Burke, K.; Ernzerhof, M. Generalized gradient approximation made simple. *Phys. Rev. Lett.* **1996**, *77*, 3865–3868.

[36] Monkhorst, H. J.; Pack, J. D. Special points for Brillouin-zone integrations. *Phys. Rev. B* **1976**, *13*, 5188–5192.

[37] Tersoff, J.; Hamann, D. R. Theory of the scanning tunneling microscope. *Phys. Rev. B* **1985**, *31*, 805–813.